

Antenna enhancing infrared photoinduced force imaging in aqueous environment with super-resolution and hypersensitivity

Jian Li,¹ Jie Pang,¹ Zhen-dong Yan,² Junghoon Jahng,³ Jin Li,¹ William Morrison,⁴ Jing Liang,¹ Qing-Ying Zhang,¹ Xing-Hua Xia^{1*}

1. State key laboratory of analytical chemistry for life science, school of chemistry and chemical engineering, Nanjing University, Nanjing 210023, China

2. College of science, Nanjing Forestry University, Nanjing 210037, China

3. Center for nanocharacterization, Korea Research Institute of Standards and Science, Daejeon 34113, Republic of Korea

4. Molecular Vista Inc., 6840 Via Del Oro, Suite 110, San Jose, CA 95119, USA.

**To whom correspondence should be addressed. E-mail: xhxia@nju.edu.cn (X.H.X)*

Keywords: Photoinduced force microscopy; aqueous environment; infrared nanospectroscopy; near-field imaging; antenna

Abstract: Tip enhanced IR spectra and imaging have been widely used in cutting-edge studies for the in-depth understanding of the composition, structure and function of interfaces at the nanoscale. However, molecular monolayer sensitivity has only been demonstrated on solid/gas interfaces. In aqueous environment, the reduced sensitivity due to strong damping of the cantilever oscillation and background IR absorption extremely limits the practical applications of tip enhanced IR nanospectroscopy. Here, we demonstrate hypersensitive nanoscale IR spectra and imaging in aqueous environment with the combination of photoinduced force (PiF) microscopy and resonant antennas. The highly confined electromagnetic field inbetween the tip end and antenna extremely amplifies the photoinduced force to the detectable level, while the excitation *via* plasmon internal reflection mode minimizes the environmental absorption. A polydimethylsiloxane (PDMS) layer (~1-2 nm thickness) functionalized on the AFM tip has been successfully identified in water with antennas of different sizes. Sampling volume of ~604 chemical bonds from PDMS was demonstrated with sub-10 nm spatial resolution confirmed by electric (E) field distribution mapping on antennas, which strongly suggests the desired requirements for interfacial spectroscopy. This platform demonstrates for the first time the application of photoinduced force microscopy in aqueous environments, providing a brand-new configuration to achieve highly enhanced nanoscale IR signals, which is extremely promising for future research of interfaces and nanosystems in aqueous environments.

Introduction

Mid-infrared (mid-IR) spectroscopy has attracted extensive attentions for interfacial studies since IR absorption of molecules arises from specific chemical bonds, allowing the analysis of molecular structures and functions without labelling or destruction.^{1,2} Recently, atomic force microscopy (AFM) based opto-mechanical force detection techniques such as photothermal induced resonance (PTIR),³⁻⁵ photoinduced force microscopy (PiFM)⁶⁻⁹ and peak force infrared (PFIR)¹⁰⁻¹² microscopy have been demonstrated to achieve IR analysis with nanoscale spatial resolution, allowing subwavelength scale investigation of chemical and physical properties of molecules. On solid/gas interfaces, the detection sensitivity has hinted at molecular monolayer level,^{3,6} which is extremely promising to reveal information about the mechanisms of interfacial processes. However, challenges arise when applying opto-mechanical force based IR techniques in aqueous environment: (1) Decrease of the sensitivity due to the damping of cantilever oscillation in water; (2) Strong background water absorption of the incident light.¹³ These intrinsic problems severely limit the range of application of AFM based IR techniques. Since aqueous environment could sustain the natural structure and function of biological molecules and also provide an environment for bio/electro-chemical reactions, the development of nanoscale IR techniques with interfacial molecular (mono)layer level sensitivity in aqueous environment is greatly desirable.

Pioneering works have been demonstrated on PTIR and PFIR by introducing attenuated total reflection (ATR) configurations,¹³⁻¹⁵ which concentrate the incident light from the substrate side and enhance the E field near the prism surface by one magnitude, allowing polymer thin film detection with thicknesses as small as 20 nm. However, in the previous works, the bulk materials entirely contribute to the opto-mechanical signals, while in interfacial studies, molecular monolayer level sensitivity is the fundamental requirement for the analysis of heterogeneous processes. Thus, groundbreaking design is yet highly desired for practical interfacial IR analysis in aqueous environment.

An antenna is a well-defined structure that can effectively confine the E field on hot spot when it is resonant with the incident light of a specific wavelength.¹⁶ Within the hot spot, IR absorption of molecules considerably increases, leading to a greatly enhanced IR response that couples with the antenna's optical response. Using back side excitation *via* "plasmon internal reflection" mode¹⁷⁻¹⁹ or ATR²⁰ mode, antenna arrays have already been used for IR analysis in the aqueous environment with high sensitivity and background absorption suppression. Thus, a combination of the back side antenna excitation and the **opto**-mechanical force based IR techniques could be a promising means to improve the sensitivity of nanoscale IR analysis in aqueous environment.

Photoinduced force (PiF) originates from both the dipole force (photoinduced electromagnetic force)²¹ and the thermal expansion-modulated van der Waals force (photoinduced thermodynamic force)²² of molecules close to the tip, which are both sensitive to interfacial molecules than bulk materials. In this study, we demonstrate that hypersensitive nanoscale IR analysis (~1-2 nm thickness of polydimethylsiloxane, PDMS) can be realized *via* antenna enhanced PiFM. The antenna-enhanced PiF spectra

follow the dissipation line shape, exhibiting the feasibility for interfacial chemical identification. With the E field dependent molecular signal, the hot spot on the antenna is mapped with spatial resolution up to sub-10 nm, suggesting a ~ 77 yoctoliter sampling volume with sub-zeptomole level detection limit. In addition, PiF spectral shape recorded on antennas with different sizes exhibits strong wavelength dependence, emphasizing the importance of suitable tuning of antenna resonance for wide spectral range nanoscale IR analysis in aqueous environment.

Results and Discussions

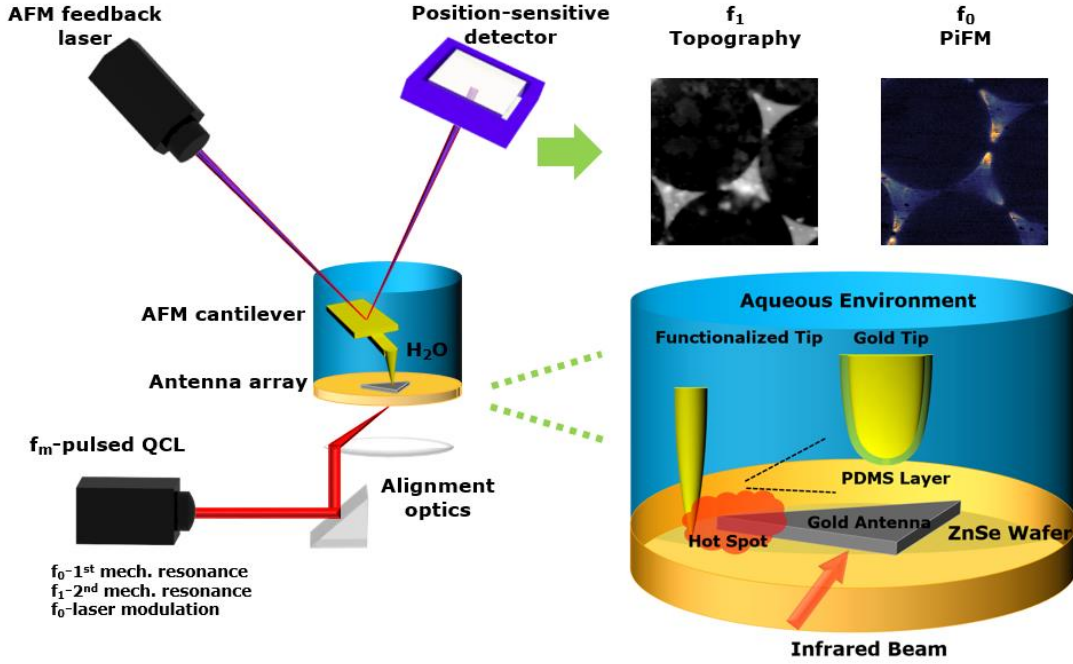


Figure 1. Schematic illustration of the antenna enhanced PiFM detection platform in aqueous environment.

The antenna enhanced PiFM detection platform in aqueous environment is schemed in Figure 1. Wafer scale Au triangle antenna array are fabricated on top of the visible to mid-IR transparent ZnSe substrate (0.5 mm thickness). An objective lens with long working distance is used to focus the non-polarized incident light from a quantum cascade laser (pulse: 44 ns). The backside illumination can minimize the absorption of aqueous solution and efficiently excite the antenna resonance. The difference between the first (f_0) and second (f_1) oscillation frequencies of the AFM tip cantilever, defined as side band modulation mode, is applied since it is demonstrated more sensitive to the force gradient. In the tapping mode detection, f_0 is used to detect the PiF signal, while f_1 is used to detect the topography. For a given molecular resonance with specific thickness d of an organic monolayer, the photoinduced thermodynamic force, the thermal expansion-modulated Van der Waals force, is dominant to the photoinduced electromagnetic force (dipole force),²³ given as:

$$\Delta F_{vDW} \propto \frac{\partial F_{vDW}}{\partial z} \sigma d \int a_{abs} |E|^2 dz \quad (1)$$

where, ΔF_{vDW} is the photoinduced force, σ is the linear thermal expansion coefficient, a_{abs} is the absorption coefficient of organic layer and E is the strength of electric field. With the near field opto-mechanical force transformation, PiF signal of the molecules inbetween the tip and antenna can be recorded with extremely high enhancement (Fig. 2).

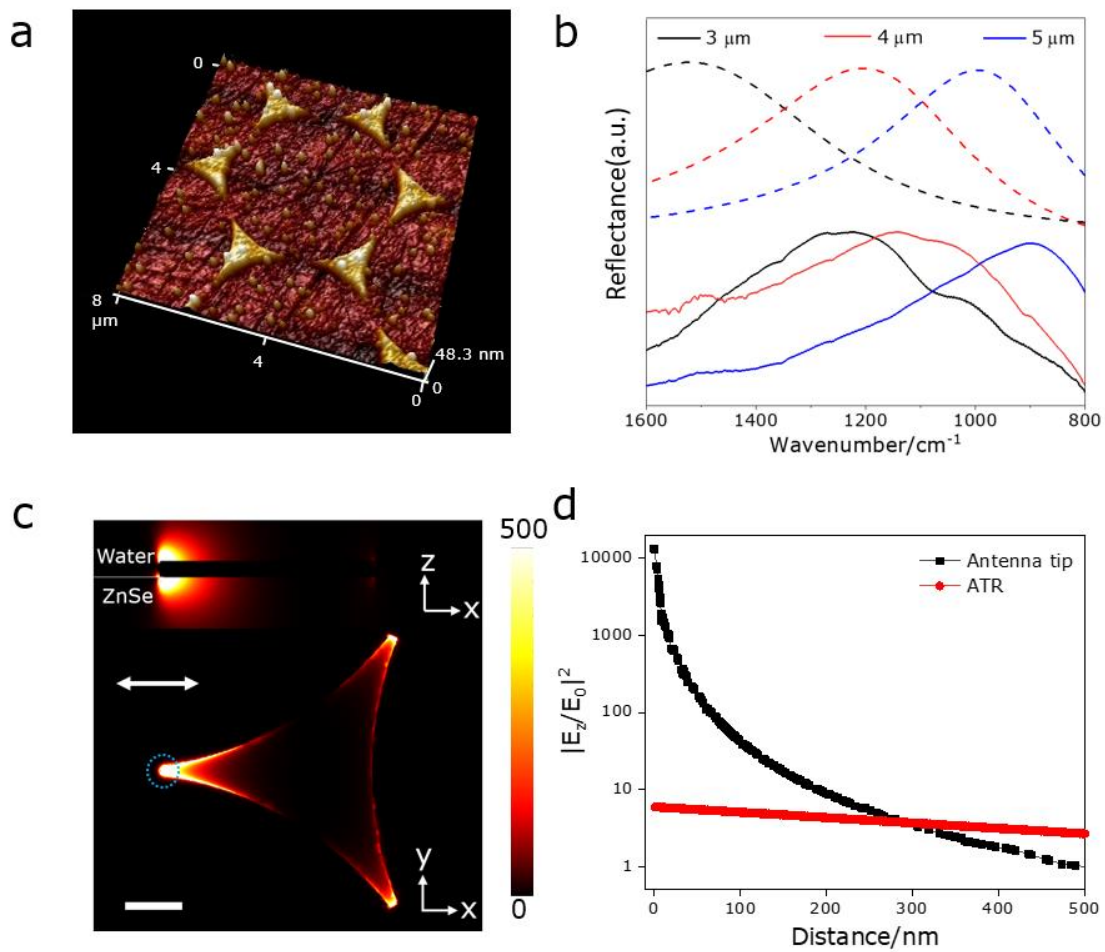


Figure 2. Properties of fabricated triangle antenna arrays. (a) AFM image of an antenna array fabricated with a mask of 5 μm polystyrene (PS) sphere; (b) Measured (solid curves) and simulated resonance spectra (normalized, dotted curves) in water of antenna arrays fabricated with masks of PS spheres of 4, 5 and 6 μm in diameter, respectively. (Substrate: ZnSe: $n=2.4$; incident angle: 12 degree); (c) Simulated $|E_z/E_0|$ distribution on an antenna fabricated with a mask of 5 μm PS sphere. (Wavenumber: 1205 cm^{-1} ; xy plane: 1 nm away in water from the antenna surface, xz plane: along the main axis of the antenna; the incident light is with s polarization as indicated by the double-head arrow with incident angle of 12 degree; scale bar in xy panel: 400 nm); (d) E_z field intensity in the sampling region with refractive index of water ($n=1.33$). Black curve: at the antenna tip as pointed by a dashed blue circle in (c). Red curve: calculation for p polarization on ZnSe with an incident angle of 45°. Wavenumber: 1205 cm^{-1} .

Figure 2a shows the AFM topography of an antenna array fabricated on a ZnSe substrate *via* nanosphere lithography with mask of 5 μm PS sphere. The highly ordered triangle shape antennas with around 50 nm height are separated with more than 100 nm distance to avoid coupling. Using of a triangle array on a flat wafer has two main advantages: (1) Triangle antennas are demonstrated to have anti-polarization properties.²⁰ Thus, non-polarized incident light can be used, which simplifies the optical alignment and avoids power reduction from a polarizer. (2) Focus of the incident beam is more

convenient than the evanescent wave achieved using an ATR prism. The detection region can be located at an arbitrary selected region on the whole wafer, while only the region on the prism center can be observed using an ATR configuration.

Figure 2b exhibits the measured and simulated antenna resonance spectra of antenna arrays with different sizes in water (backside excitation with 12 degree of incident angle). For simplification, the simulation only using the *s*-polarization along the main axis on single antenna is shown in Figure 2c. As is clearly seen, the simulated antenna resonance correlates well with the experimental data, the slight peak position shift could be owing to the shape and size variations of the real antenna with the model. As compared to the antenna resonance in air, the resonance of antenna with the same size red-shifts around 100~200 cm^{-1} (Figure S1) because of the larger refractive index of water ($n=1.33$) than air ($n=1$). By changing the PS sphere from 4 μm to 6 μm , the antenna resonance can be tuned from $\sim 1205 \text{ cm}^{-1}$ to $\sim 900 \text{ cm}^{-1}$, crossing wide spectral range for the IR detection. In addition, we find that the incident angle has minute influence on the resonance peak position by simulation (Figure S2), suggesting that the effect of different incident angle owing to objective lens can be minimized.

The better confinement of E-field makes the antenna array a highly advantageous alternative to an ATR configuration. As the simulations in Figure 2c and Figure S3 show, when the plasmon resonance is excited by the light incident from the substrate side, extremely confined and enhanced E-field is generated at the tip end of the antenna in the aqueous environment, providing unique opportunities to increase the light matter interaction in such a hot spot region. The E field enhancement is also compared with the normally used ATR configuration (Figure 2d) in the sampling region. For the ATR excitation with 45 degree *p*-polarized light illumination, the intrinsic E_z field enhancement is only 5.9, while on the antenna tip, the enhancement is more than 1000 times of that on the ATR prism surface. Since PiF is proportional to $|E|^2$, the on antenna detection is expected to be a couple of orders of magnitude higher than on ATR prism. In addition, the E field is only confined close to the antenna surface within less than 50 nm, while in ATR configuration the field would penetrate more than 500 nm distance, suggesting the extremely near field sensitivity of the antenna induced E-field enhancement for the detection. These advantages make the antenna array a better platform for highly sensitive PiFM measurements, especially for interfacial studies.

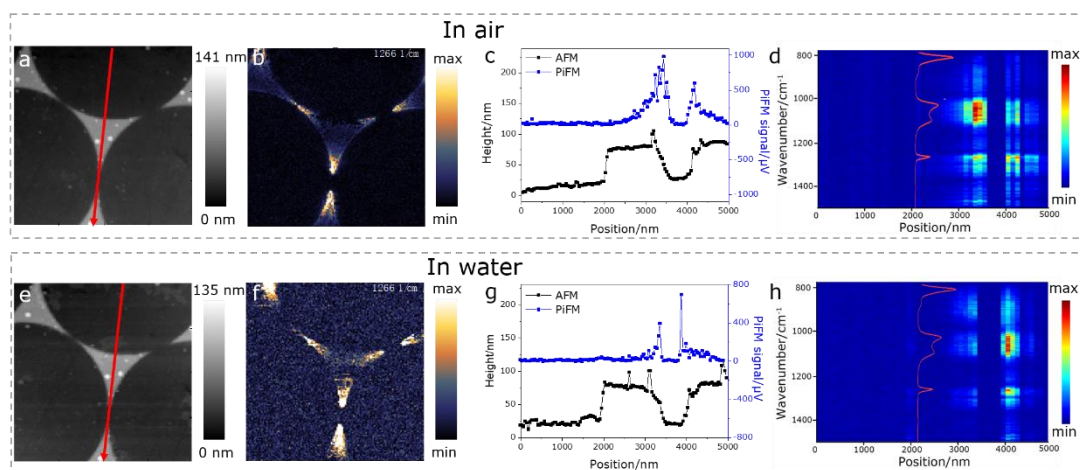


Figure 3. PiFM measurements on an antenna fabricated with 5 μm PS sphere. (a) and (e): AFM images of the same region recorded in air and water, respectively. Scale bar: 1 μm . (b) and (f): PiF images of the same region recorded at 1266 cm^{-1} simultaneously with (a) and (e), respectively. (c) and (g): Signals along the red arrows of the topography (black curve) and PiFM images (blue curve). (d) and (i): Corresponding spatio-spectral transection along the red arrows. Spectra were obtained in 5 s with 1 cm^{-1} spectral resolution, with 100 nm separation.

In most of the proof-of-concept demonstrations for in aqueous nanoscale IR analysis, patterned polymer films or aggregates of peptides were prepared on substrates as samples, which are relatively thick that are far from the molecular monolayer level. Meanwhile, these samples are normally with irregular geometry and unclear margin, making it difficult to determine the spatial resolution. In our work, a reverse strategy for sampling is applied. The PDMS layer on the commercial PtIr AFM tip is used as the target, which is naturally functionalized on the tip in the packaging box with the thickness $\sim 1\text{--}2$ nm.^{24, 25} Such sampling strategy has several advantages: (1) Sample variation on different detection region could be eliminated, making it reliable to compare the signal enhancement on different positions and different antennas; (2) PDMS has four characteristic IR peaks at 1266 cm^{-1} , 1100 cm^{-1} , 1025 cm^{-1} and 816 cm^{-1} (dielectric function shown in Figure S4), which overlap well with the resonance of the applied antenna arrays; (3) PDMS has relatively high absorption coefficient and large thermal expansion coefficient which are expected to induce strong photoinduced thermodynamic force.

We first performed PiF studies on the antenna array fabricated with 5 μm PS sphere in air and water in the same region. The f_0 and f_1 frequencies of the cantilever shift from 262.2 kHz and 1653 kHz to 128.2 kHz and 875.8 kHz, respectively, due to the oscillation damping of the cantilever in water, accompanied by a huge Q factor decrease. The exact Q decrease is difficult to estimate because once in liquid, the resonance peak used becomes too asymmetric and unpredictable to effectively measure a full width at half maximum. Figure 3a and 3e show the AFM images of the same region recorded in air and water, respectively. The similar geometry and defects suggest that the detection region are on the same antenna. As shown in Figure 3b and 3f, the simultaneously recorded PiF signals at 1266 cm^{-1} strongly exhibit position dependent optical responses. Since the PDMS layer is modified on AFM tip, the artifact due to the variation in molecules amount and geometry can be excluded, the observed signal can be concluded from the E field induced light/matter interaction at the different position of the antenna. According to formula (1), the measured PiF signal mainly arises from the Van der Waals force induced by the PDMS expansion, which is proportional to the localized E field intensity. Thus, despite the tapping mode operation induced gap size variation and heat diffusion in water, the collected PiF image can be qualitatively used to image the E field distribution on the antenna. As demonstrated at different wavenumbers (Figure 3f and S5), the antenna tip end has the highest PiF signal, which is also in agreement with the simulated E field distribution as shown in Figure 2c.

We further collected the PiF spectra of PDMS on the antenna along the red arrows indicated in Figure 3a and 3e, the relative AFM and PiF signals in images were

extracted and plotted in Figure 3c and 3g for comparison, respectively. The position dependent PiF spectra are shown in Figure 3d and 3h with the same position coordinate of Figure 3c and 3f. The PiF spectra of the tip clearly show the molecular features of PDMS at 1266 cm^{-1} , 1100 cm^{-1} and 1020 cm^{-1} , which are in agreement with the far field band characteristics (red line in Figure 3d and 3h). Because the PDMS layer is expected as 1-2 nm thick, the hypersensitivity in aqueous environment can be achieved in our platform, which is an important step forward for nanoscale IR analysis. The observed spectra follow the dissipative lineshape (photoinduced thermodynamic force) rather than the dispersive lineshape (photoinduced electromagnetic force) of PDMS or the antenna resonance,²³ suggesting that the absorption induced Van der Waals force modulation is dominant inbetween the tip-PDMS-antenna junction. These distinct spectral features suggesting that the proposed method can be used for the nanoscale chemical identification. In addition, the PiF spectral signal is extremely strong near the tip end of the antenna and decrease rapidly when the detection position moves to the antenna surface, which is in agreement with the recorded PiF images and extracted E_z strength in the simulation (Figure S6), confirming the origin of the PiF images as the antenna enhanced thermal expansion of target molecules.

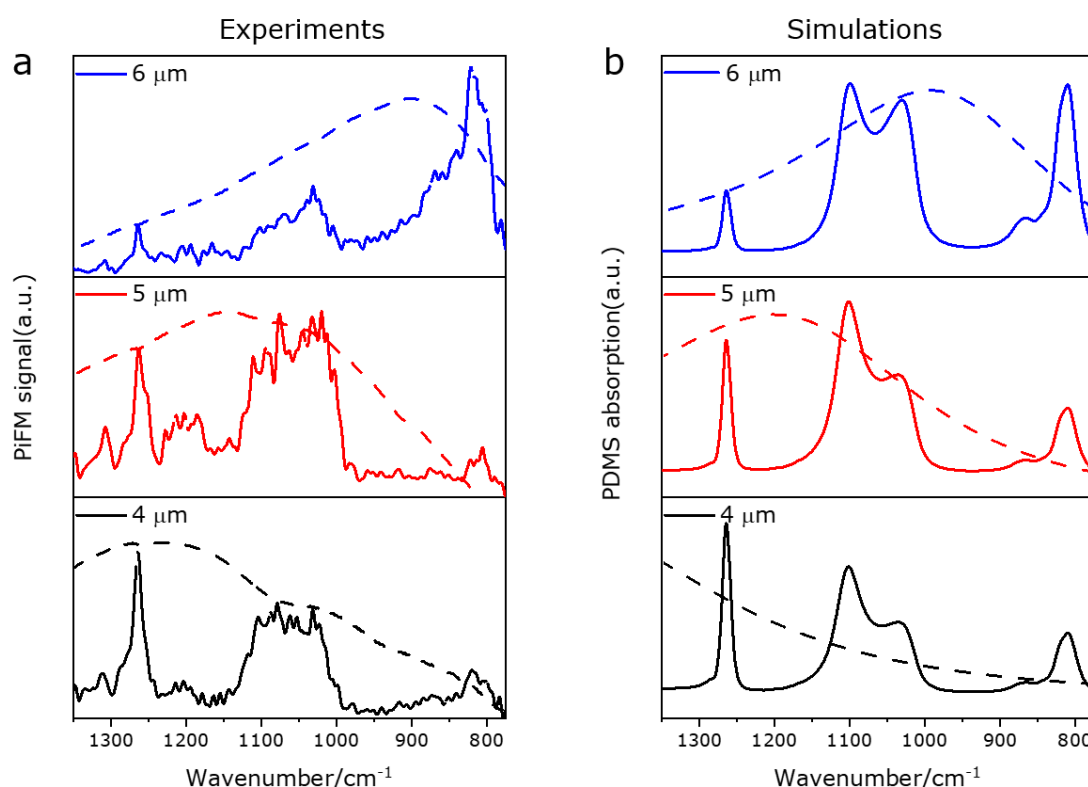


Figure 4. PiF spectra on antenna fabricated with PS spheres of different sizes. (a) Measured PiFM spectra and (b) simulated PDMS absorption profiles at the tip end of antennas fabricated with PS spheres of different sizes. Dashed lines show the relative antenna resonance profiles for comparison.

We then performed the nanoscale IR spectra and imaging on the antenna arrays fabricated with PS sphere diameters of 4 μm and 6 μm . The acquired AFM and PiFM images are of high quality and the IR spectra are successfully recorded with position (Figure S8-S11), demonstrating the great feasibility and reproducibility of our antenna enhanced PiFM approach for the in aqueous nanoscale IR analysis with hypersensitivity. Since PDMS has 4 characteristic peaks within the antenna's resonance region, the PiFM results provide a unique way to control the coupling between different molecular vibrations within the antenna resonances, which is hard to perform *via* s-SNOM due to the huge scattering background of the antenna.^{26, 27} Figure 4(a) exhibits the measured PiFM spectra of PDMS at the tip end of antenna fabricated with different sized PS spheres. Horizontally, on antenna fabricated with 4 μm PS sphere with resonance at 1205 cm^{-1} , the peak at 1266 cm^{-1} is much higher than at 816 cm^{-1} , which is reversed on antenna fabricated with 6 μm PS spheres with resonance at 898 cm^{-1} that the peak at 1266 cm^{-1} is much lower than at 816 cm^{-1} . This is mainly because that on the same antenna, the E field is much confined when the wavelength is close to the antenna resonance, inducing the higher absorption of the molecular vibration more close to the antenna resonance. Although this phenomenon is widely accepted and exhibited in the far field experiments, our work is the first near field demonstration in aqueous environment for the resonance dependent peak enhancement of molecules on the same antenna. Meanwhile, the enhancement of the same peak with different antenna resonances is longitudinally compared. With the increase of antenna sizes, the antenna resonance peaks shift from 1205 cm^{-1} to 898 cm^{-1} . The strength of the peak at 1266 cm^{-1} decreases due to the gradually mismatch with the antenna resonance, while the peak at 816 cm^{-1} increases since it couples better with the longer wavelength resonance. Interestingly, for the adjacent peaks at 1100 cm^{-1} and 1020 cm^{-1} , the relative strength of the PiF signals exhibit the similar tendency. These results are in great agreement with the simulation of PDMS absorption below the AFM tip (details in supporting information), demonstrating the effective coupling between antenna, tip and PDMS molecules. Notably, we have also performed the PiFM measurements on a clean ZnSe substrate in water. However, no PiFM signal can be observed, further emphasizing the importance of antenna resonance for the effective detection in our platform.

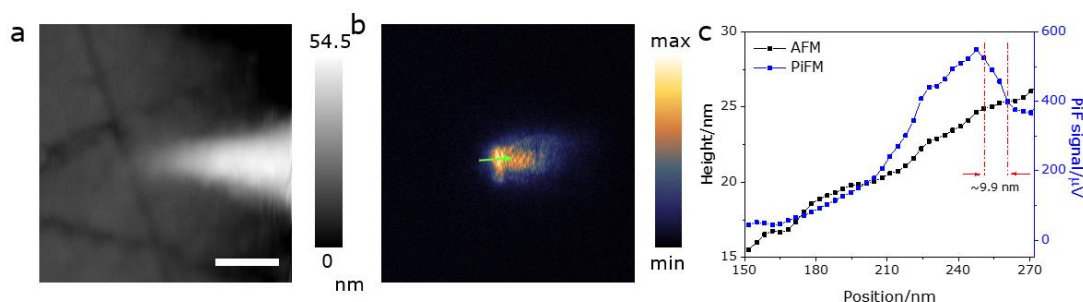


Figure 5. PiFM measurements with high spatial resolution. (a) AFM image of tip end of antenna fabricated with 6 μm PS sphere recorded in water. Scale bar: 200 nm. (b) PiF images of the same region recorded at 1100 cm^{-1} simultaneously with (a). (c)

Signals along the green arrow of topography (black curve) and PiFM images (blue curve).

A detailed image on the tip end of an antenna fabricated with 6 μm PS sphere was recorded in water to verify the spatial resolution of our platform (Figure 5a and 5b). As indicated in the simulation, the tip end of antenna has the highest E field enhancement. Thus, the minimum spatial distance that could clearly distinct this end can be defined as the spatial resolution, which is benefiting from the PDMS functionalization to eliminate the sample artifact. According to the trace line, the tip end with the highest PiF signal can be obviously distinguished, while the antenna height still gradually increases. From that optical tip end, PiF signal would decrease as the detection position moves away from that point. Thus, the spatial resolution of our platform can be around 9.9 nm in this experiment for a clear optical signal stage, which is very comparable with the PiFM detection of monolayers in air.⁶

We then estimate the resolution and sensitivity of our platform. Since the thickness of PDMS layer on AFM tip is $\sim 1\text{-}2$ nm, the detection volume is calculated around 7.69×10^{-23} L underneath the AFM tip with the 9.9 nm spatial resolution. Assuming that PDMS has the similar density of bulk materials (965 g/L), the monomer unit of PDMS (74 g/mol) can be calculated as ~ 604 at sub-zeptomole level, which is 2 orders higher than the best existing PTIR results¹³ and is comparable to the molecular monolayer detection limit of PiFM in air. Thus, the proposed antenna enhanced PiFM strategy has been demonstrated with extreme sensitivity and super resolution in an aqueous environment.

Conclusion

In summary, we have proposed a novel nanoscale IR spectra and imaging method in aqueous environment based on the combination of PiFM and a mid-IR resonant antenna array. Our approach allows hundreds molecules level detection with sub-10 nm spatial resolution in aqueous environment, which meets the sensitivity and resolution requirements for the fundamental interfacial studies. With the enhanced PiF signal of PDMS, the E-field distribution on the antenna is clearly imaged, while with the resonance-dependent PiF signal, the chemical identification of PDMS has been successfully demonstrated. This work has improved the performance of force based nanoscale IR techniques, which we hope eventually to be broadly used in interfacial studies of chemical, biological, and electrochemical processes.

Reference

- [1] Li, J.; Zheng, B.; Zhang, Q. W.; Liu, Y.; Shi, C. F.; Wang, F. B.; Wang, K.; Xia, X. H. Attenuated Total Reflection Surface-Enhanced Infrared Absorption Spectroscopy: A Powerful Technique for Bioanalysis. *J. Anal. Test.* **2017**, *1*, 8.
- [2] Bao, W. J.; Li, J.; Li, J.; Zhang, Q. W.; Liu, Y.; Shi, C. F.; Xia, X. H. Au/ZnSe-Based

Surface Enhanced Infrared Absorption Spectroscopy as A Universal Platform for Bioanalysis. *Anal. Chem.* **2018**, *90*, 3842-3848.

[3] Lu, F.; Jin, M.; Belkin, M. A. Tip-Enhanced Infrared Nanospectroscopy *via* Molecular Expansion Force Detection. *Nat. Photo.* **2014**, *8*, 307.

[4] Dazzi, A.; Craig, B. P. AFM-IR: Technology and Applications in Nanoscale Infrared Spectroscopy and Chemical Imaging. *Chem. Rev.* **2016**, *117*, 5146-5173.

[5] Dazzi, A.; Prazeres, R.; Glotin, F.; Ortega, J. M. Local Infrared Microspectroscopy with Subwavelength Spatial Resolution with An Atomic Force Microscope Tip Used as A Photothermal Sensor. *Opt. Lett.* **2005**, *30*, 2388-2390.

[6] Li, J.; Jahng, J.; Pang, J.; Morrison, W.; Li, J.; Lee, E.S.; Xu, J.J.; Chen, H.Y.; Xia, X.H. Tip-Enhanced Infrared Imaging with Sub-10 nm Resolution and Hypersensitivity. *J. Phys. Chem. Lett.* **2020**, *11*, 1697-1701.

[7] Nowak, D.; Morrison, W.; Wickramasinghe, H.K.; Jahng, J.; Potma, E.; Wan, L.; Ruiz, R.; Albrecht, T.R.; Schmidt, K.; Frommer, J.; Sanders, D.P. Nanoscale Chemical Imaging by Photoinduced Force Microscopy. *Sci. Adv.* **2016**, *2*, e1501571.

[8] Jahng, J.; Son, J.G.; Kim, H.; Park, J.; Lee, T.G.; Lee, E.S. Direct Chemical Imaging of Ligand-Functionalized Single Nanoparticles by Photoinduced Force Microscopy. *J. Phys. Chem. Lett.* **2020**, *11*, 5785-5791.

[9] Li, J.; Shen, Q.; Li, J.; Liang, J.; Wang, K.; Xia, X. H. *d-sp* Interband Transition Excited Carriers Promoting the Photochemical Growth of Plasmonic Gold Nanoparticles. *J. Phys. Chem. Lett.* **2020**, *11*, doi.org/10.1021/acs.jpcclett.0c02325

[10] Wang, L.; Wang, H.; Wagner, M.; Yan, Y.; Jakob, D.S.; Xu, X.G. Nanoscale Simultaneous Chemical and Mechanical Imaging *via* Peak Force Infrared Microscopy. *Sci. Adv.* **2017**, *3*, e1700255.

[11] Jakob, D.S.; Wang, H.; Zeng, G.; Otzen, D.E.; Yan, Y.; Xu, X. Peak Force Infrared-Kelvin Probe Force Microscopy. *Angew. Chem. Int. Ed.* **2020**, <https://doi.org/10.1002/ange.202004211>.

[12] Wang, L.; Jakob, D.S.; Wang, H.; Apostolos, A.; Pires, M.M.; Xu, X.G. Generalized Heterodyne Configurations for Photoinduced Force Microscopy. *Anal. Chem.* **2019**, *91*, 13251-13259.

[13] Jin, M.; Lu, F.; Belkin, M.A. High-Sensitivity Infrared Vibrational Nanospectroscopy in Water. *Light Sci. Appl.* **2017**, *6*, e17096-e17096.

[14] Ramer, G.; Ruggeri, F.S.; Levin, A.; Knowles, T.P.; Centrone, A. Determination of Polypeptide Conformation with Nanoscale Resolution in Water. *ACS Nano* **2018**, *12*, 6612-6619.

[15] Wang, H.; Janzen, E.; Wang, L.; Edgar, J.H.; Xu, X.G. Probing Mid-Infrared Phonon Polaritons in the Aqueous Phase. *Nano Lett.* **2020**, *20*, 3986-3991.

[16] Neubrech, F.; Huck, C.; Weber, K.; Pucci, A.; Giessen, H. Surface-Enhanced Infrared Spectroscopy Using Resonant Nanoantennas. *Chem. Rev.* **2017**, *117*, 5110-5145.

[17] Adato, R. and Altug, H. In-situ Ultra-Sensitive Infrared Absorption Spectroscopy of Biomolecule Interactions in Real Time with Plasmonic Nanoantennas. *Nat. Commun.* **2013**, *4*, 2154.

- [18] Limaj, O.; Etezadi, D.; Wittenberg, N.J.; Rodrigo, D.; Yoo, D.; Oh, S.H.; Altug, H. Infrared Plasmonic Biosensor for Real-Time and Label-Free Monitoring of Lipid Membranes. *Nano Lett.* **2016**, *16*, 1502-1508.
- [19] Pfitzner, E.; Seki, H.; Schlesinger, R.; Ataka, K.; Heberle, J. Disc Antenna Enhanced Infrared Spectroscopy: From Self-Assembled Monolayers to Membrane Proteins. *ACS Sens.* **2018**, *3*, 984–991.
- [20] Li, J.; Yan, Z.; Li, J.; Wang, Z.; Morrison, W.; Xia, X.H. Antenna Array-Enhanced Attenuated Total Reflection IR Analysis in an Aqueous Solution. *Nanoscale* **2019**, *11*, 18543-18549.
- [21] Jahng, J.; Brocious, J.; Fishman, D.A.; Huang, F.; Li, X.; Tamma, V.A.; Wickramasinghe, H.K.; Potma, E.O. Gradient and Scattering Forces in Photoinduced Force Microscopy. *Phys. Rev. B* **2014**, *90*, 155417.
- [22] Jahng, J.; Potma, E.O.; Lee, E.S. Tip-Enhanced Thermal Expansion Force for Nanoscale Chemical Imaging and Spectroscopy in Photoinduced Force Microscopy. *Anal. Chem.* **2018**, *90*, 11054-11061.
- [23] Jahng, J.; Potma, E.O.; Lee, E.S. Nanoscale Spectroscopic Origins of Photoinduced Tip–Sample Force in the Midinfrared. *Proc. Natl. Acad. Sci. U.S.A* **2019**, *116*, 26359-26366.
- [24] Jahng, J.; Yang, H.; Lee, E.S. Substructure Imaging of Heterogeneous Nanomaterials with Enhanced Refractive Index Contrast by Using a Functionalized Tip in Photoinduced Force Microscopy. *Light Sci. Appl.* **2018**, *7*, 1-9.
- [25] Sirghi, L.; Kylián, O.; Gilliland, D.; Ceccone, G.; Rossi, F. Cleaning And Hydrophilization of Atomic Force Microscopy Silicon Probes. *J. Phys. Chem. B* **2006**, *110*, 25975–25981.
- [26] O’Callahan, B.T.; Hentschel, M.; Raschke, M.B.; El-Khoury, P.Z.; Lea, A.S. Ultrasensitive Tip-and Antenna-Enhanced Infrared Nanoscopy of Protein Complexes. *J. Phys. Chem. C* **2019**, *123*, 17505-17509.
- [27] Muller, E.A.; Pollard, B.; Bechtel, H.A.; Adato, R.; Etezadi, D.; Altug, H.; Raschke, M.B. Nanoimaging and Control of Molecular Vibrations Through Electromagnetically Induced Scattering Reaching the Strong Coupling Regime. *ACS Photonics* **2018**, *5*, 3594-3600.

TOC

